Sensory experience controls dendritic structure and behavior by distinct pathways involving degenerins

Sharon Inberg, Yael Iosilevskii and Benjamin Podbilewicz*

Department of Biology, Technion-Israel Institute of Technology, 3200003 Haifa, Israel

* Corresponding author
Department of Biology, Emerson Building, Room 4-31
Technion-Israel Institute of Technology, 3200003 Haifa, Israel
Tel +972 4 8293454
Email: podbilew@technion.ac.il

Author Contributions: SI and BP conceived and designed the experiments. SI performed the experiments. YI conceived, designed and performed some behavioral and structural experiments. SI, YI and BP analyzed the data and wrote the paper.

Competing Interest Statement: None

Classification: Biological Sciences. Neuroscience

Keywords: Dendritic plasticity, *Caenorhabditis elegans,* Epithelial sodium channels (degenerins)

This PDF file includes:

Main Text
Figures 1 to 6

Abstract

Dendrites are crucial for receiving information into neurons. Sensory experience affects the structure of these tree-like neurites, which, it is assumed, modifies neuronal function, yet the evidence is scarce, and the mechanisms are unknown. To study whether sensory experience affects dendritic morphology, we use the *Caenorhabditis elegans'* arborized nociceptor PVD neurons, under natural mechanical stimulation induced by physical contacts between individuals. We found that mechanosensory signals induced by conspecifics affect the dendritic structure of the PVD. Moreover, developmentally isolated animals show a decrease in their ability to respond to harsh touch. The structural and behavioral plasticity following sensory deprivation are functionally independent of each other and are mediated by an array of evolutionarily conserved mechanosensory amiloride-sensitive epithelial sodium channels (degenerins). Our genetic results, supported by optogenetic, behavioral, and pharmacological evidence, suggest an activity-dependent homeostatic mechanism for dendritic structural plasticity, that in parallel controls escape response to noxious mechanosensory stimuli.

Significance Statement

Little is known about how neuronal activity and sensory experience influence the structure and function of dendritic trees. Furthermore, how dendritic structures affect neuronal functions remains to a large extent a mystery despite their fundamental functions in neuronal sensory and synaptic activities in health and diseases. Here we show that complex dendritic trees of the nociceptive and proprioceptive PVD neuron in *C. elegans* display a dynamic nature where they undergo pronounced dendritic modifications during adulthood. These modifications are determined by the received sensory signals generated by conspecific worms on the plate. We revealed functions for degenerins/Epithelial sodium channels in this phenomenon, using genetic and optogenetic approaches. We found that the degenerin MEC-10 acts cell autonomously to translate environmental mechanical signals into structural and functional modifications in the PVD.

Main Text

Introduction

The general structure of the nervous system has been known for over a century. Groundbreaking studies on synaptic plasticity and its underlying mechanisms have shown that before birth and in adult animals, neuronal activity is needed for synaptic remodeling (Fox & Wong, 2005, Goodman & Shatz, 1993, Katz & Shatz, 1996, Wiesner, Bilodeau et al., 2020, Zuo, Yang et al., 2005). In contrast, the molecular mechanisms responsible for structural remodeling of dendritic trees, as a result of different sensory inputs (experience), especially during adulthood, are less understood (Kolb & Whishaw, 1998, Tavosanis, 2012, Wong & Ghosh, 2002).

Mechanistic understanding of experience-dependent structural plasticity is primarily focused on activity sensation by calcium channels and N-methyl-D-aspartate (NMDA) receptors. These are known to induce downstream signaling cascades affecting, among others, the Rho family of small GTPases, calcium metabolism and microtubule stability (Ghiretti, Moore et al., 2014, Sin, Haas et al., 2002, Vaillant, Zanassi et al., 2002, Zhou, Hong et al., 2006). Several neurological conditions including autism, Down syndrome, fragile X syndrome, and schizophrenia are characterized by abnormal dendritic spine structures (Hu, Huang et al., 2020, Huebschman, Corona et al., 2020, Jan & Jan, 2010, Tendilla-Beltran, Antonio Vazquez-Roque et al., 2019). Uncovering the molecular basis of dendritic tree instability during development and adulthood, may shed light on neurological disease mechanisms and elucidate their behavioral phenotypes.

The dendrite morphology of the *Caenorhabditis elegans'* PVD bilateral neurons is composed of repetitive, stereotypical and spatially organized structural units that resemble candelabra (Fig. 1A), making it a useful platform to study dendritic morphogenesis (Oren-Suissa, Hall et al., 2010). While some of the genetically-programmed molecular mechanisms responsible for the morphogenesis and regeneration of PVD's dendritic trees are known (Dong, Liu et al., 2013, Dong, Shen et al., 2015, Inberg, Meledin et al., 2019, Kravtsov, Oren-Suissa et al., 2017, Oren-Suissa, Gattegno et al., 2017, Oren-Suissa et al., 2010, Salzberg, Diaz-Balzac et al., 2013, Salzberg, Ramirez-Suarez et al., 2014, Smith, Watson et al., 2010), the influence of nurture, e.g. sensory experience, on its structure and function during development and in adulthood remain unexplored. The PVD mediates three sensory modalities (reviewed in (Goodman & Sengupta, 2019)): response to harsh mechanical stimuli (nociception) (Chatzigeorgiou, Yoo et al., 2010), response to low temperatures (Chatzigeorgiou et al., 2010) and proprioception (Albeg, Smith et al., 2011, Tao, Porto et al., 2019). While the PVD response to low temperatures is mediated by transient receptor potential (TRP) channels (Chatzigeorgiou et al., 2010), nociception and proprioception are mediated by degenerins/epithelial Na^+ channels (DEG/ENaCs) expressed in the PVD

(Chatzigeorgiou et al., 2010, Husson, Costa et al., 2012), which form homo- and hetero-trimers and are involved in force sensing. In mammals, some DEG/ENaCs such as ASIC1a participate in synaptic plasticity and cognitive functions such as learning and memory (Baldin, Barth et al., 2020, Bianchi & Driscoll, 2002, Chen, Bharill et al., 2015, Gillespie, 2001, Gobetto, Gonzalez-Inchauspe et al., 2021, Hill & Ben-Shahar, 2018, Mango & Nistico, 2020, Welsh, Price et al., 2002). As sensory and social isolation affect the behavior and fitness of diverse animals (Bailey & Moore, 2018, Kuhlman, O'Connor et al., 2014, Wilbrecht, Holtmaat et al., 2010, Yu & Zuo, 2011), including primates (Harlow, Dodsworth et al., 1965), studying adult nematode somatosensory neurons can reveal possibly-conserved mechanisms of dendritic plasticity, which are induced by sensory stimuli.

In gentle touch circuits, which are distinct from nociception (Chalfie & Sulston, 1981, Li, Kang et al., 2011, Oren-Suissa et al., 2010), Rose and colleagues (Rose, Sangha et al., 2005) found that deprivation of mechanosensory stimulation generated by colliding conspecifics in the growing plate, resulted in modified glutamatergic signaling and reduced response to tap stimulation. Here, we adapted this mechanosensory stimulation paradigm (Rose et al., 2005), where the crowded worms are thought to represent the natural ‘default’ enriched mechanosensory state, to look into nociceptive circuits and identify the mechanism that couples mechanosensory experience to structural and functional dendritic plasticity. We focused on how mechanosensory experience, perceived through DEG/ENaCs, affects structural plasticity of the PVD dendritic trees in adult *C. elegans*, and whether this entails behavioral consequences. We find that mechanosensory experience not only alters the PVD’s dendritic structure in the adults, but also affects associated behavioral outputs. However, and in contrast to the prevalent hypothesis, these structural and behavioral properties are not correlated.

Results

Sensory isolation induces behavioral plasticity

Rose and colleagues (Rose et al., 2005) has shown that isolation of wildtype (WT) *C. elegans* causes a decreased response to gentle touch circuits when comparing to worms raised in a crowded setting. We utilized a similar paradigm to study nociception, a behavior associated with PVD neuron activation (Oren-Suissa et al., 2010, Way & Chalfie, 1988), using a behavioral assay that registers escape following prodding with a platinum wire (harsh touch assay; Fig. 1A) (Chalfie & Sulston, 1981, Li et al., 2011, Oren-Suissa et al., 2010). To study whether mechanosensory deprivation affects the nociceptive functions of the PVD, we isolated embryos into single plates where they grew 72 h to adulthood and compared their behavioral response to harsh touch against same-aged adults that were grown on crowded plates (Fig. 1B). We found that ~40% of isolated WT animals responded to harsh touch, compared with ~80% of animals grown

128 in crowded plates (Fig. 1C). To test whether gentle touch neurons are involved in this
129 behavioral difference, we studied *mec-4(e1611)* mutants, in which gentle touch neurons
130 are degraded (Caneo, Julian et al., 2019, Driscoll & Chalfie, 1991, Hedgecock, Sulston
131 et al., 1983, Li et al., 2011, Suzuki, Kerr et al., 2003), and obtained similar results (Fig.
132 1C). Given that *mec-4(e1611)* exhibits the same experience-dependent behavioral
133 plasticity as WT, we conclude that this phenomenon is independent from the *mec-4*
134 gentle-touch neurons. As a negative control, we used *mec-3(e1338)* mutants, that are
135 harsh-touch-insensitive (Way & Chalfie, 1988) and found no responses for both groups
136 (Fig. 1C). Thus, isolation reduces the response to noxious stimuli, in a process that is
137 independent of gentle touch circuits.

138 To determine whether the effect of isolation on nociception is related to the
139 mechanosensory deficit itself (like friction (Shi, Luke et al., 2016) and collisions
140 (Chatzigeorgiou et al., 2010), in contrast to chemosensory stimuli, we used the *mec-4*
141 strain to compare responses of isolated worms to responses of isolated worms grown in
142 the presence of glass beads (resembling a method used by (Sawin, Ranganathan et al.,
143 2000)). Worms grown in isolation with beads had a similar response compared to
144 animals grown in crowded plates (Fig. S1A). While the beads are sufficient to increase
145 isolated animals' responses, they do not fully recapitulate the crowded state (Fig. S1A).
146 To study whether the effect was chemosensory-mediated, we tested plates pre-
147 stimulated with pheromones as well as *osm-6* mutants (defective in olfactory sensory
148 cilia (Collet, Spike et al., 1998)). We found that isolation induced a reduction in the
149 response to harsh touch, regardless of plate 'odor' (Fig. 1D) or chemosensory function
150 (Fig. S1B). We note that the chemosensory defective *osm-6* mutants also have a
151 defective ciliated mechanosensory PDE neuron (Collet et al., 1998) (which mediates
152 posterior harsh touch responses (Li et al., 2011)). These results suggest that adult
153 worms display a behavioral plasticity in PVD-related harsh touch circuits, which is
154 dependent on mechanosensory experience, and is independent of the PDE neuron,
155 olfactory and gentle touch neurons.

156

157 **MEC-10 and other mechanosensory channels mediate isolation-induced**
158 **behavioral plasticity before adulthood**

159 To study the genetic mechanisms behind the nociceptive response plasticity, we
160 performed a candidate gene screen for degenerins (DEG/ENaC) and transient receptor
161 potential (TRP) channels that are expressed in the PVD, where degenerins mediate
162 mechanosensation and proprioception, while TRPs sense low temperatures. In all these
163 signal transduction pathways some of the outcomes are behavioral responses
164 (Chatzigeorgiou et al., 2010, Huang & Chalfie, 1994). We found that the WT-like
165 isolation-induced reduction in harsh touch response was also present in *degt-1*
166 DEG/ENaC and *gtl-1* TRP channel mutants, suggesting that these channels are not
167 directly involved in behavioral plasticity following isolation (Fig. 1E). In contrast, for *del-*

168 *1*, *asic-1* and *mec-10* DEG/ENaC mutants the difference between isolated and crowded
169 conditions was undetectable, indicating that they are required for such behavioral
170 plasticity. Interestingly, while the harsh touch response of *asic-1* mutants was
171 consistently high, and similar to crowded WT worms, the response for *mec-10* mutants
172 was consistently low, similar to isolated WT animals, regardless of sensory experience
173 (Fig. 1E). To test whether the response to harsh touch is dependent on DEG/ENaC
174 activity, we used the DEG/ENaC blocker amiloride (Ben-Shahar, 2011, Bianchi &
175 Driscoll, 2002) on WT worms that were grown in crowded plates. We found that the
176 response to harsh touch was not affected by continuous growth in the presence of
177 amiloride (Fig. S1C). This result possibly supports the idea that different amiloride-
178 sensitive epithelial sodium channels may have positive and negative effects on the
179 response to harsh touch, which are masked by global inhibition (Fig. 1E). This is further
180 evident by the plasticity consequences of some double and triple DEG/ENaC mutant
181 combinations, which are difficult to align into an epistatic genetic model (Fig. S8).

182 The DEG/ENaC MEC-10 is expressed in the PVD and responds to
183 mechanosensory signals (Chatzigeorgiou et al., 2010) including shear forces (Shi et al.,
184 2016, Shi, Mutchler et al., 2018). Since crowded *mec-10* mutants seem isolated-like in
185 their behavioral response (Fig. 1E), we asked how *mec-10* mediates the behavioral
186 plasticity in crowded conditions. To test whether the activity of MEC-10 is required
187 autonomously in the PVD, we expressed MEC-10 under a PVD-specific promoter in a
188 *mec-10* mutant background (Oren-Suissa et al., 2010, Tsalik, Niacaris et al., 2003). We
189 found that expression of MEC-10 in the PVD rescues the low response to harsh touch in
190 crowded *mec-10* mutants, indicating that it acts cell autonomously to modulate
191 behavioral plasticity (Fig. 1F).

192 To determine whether isolation affects the response to harsh touch during
193 development or in adults, we isolated crowded-raised young adults for 24 h and found
194 no difference in their response to harsh touch (Fig. 1G). Thus, isolation-induced
195 reduction in mechanosensation is determined before young adults, is PVD cell-
196 autonomous, and *mec-10*-dependent.

197 **Experience affects PVD morphology via *mec-10* in adulthood**

198 Sensory experience (such as stimuli deprivation) is known to drive synaptic plasticity in
199 the nervous system (Alvarez & Sabatini, 2007, Fox & Wong, 2005, Zuo et al., 2005).
200 However, little is known about the effects of mechanosensory deprivation on the
201 architecture of sensory neurons. To study whether reduced mechanosensory
202 experience can alter the dendritic structure of the PVD we followed the isolated growth
203 paradigm (Fig. 1B) and examined two morphological features of the PVD (Fig. 2A): The
204 fraction of ectopic (excessive, disordered) branches out of non-ectopic branches (those
205 that form the 'ideal' candelabrum), and the percentage of straight 4th order (quaternary)
206 branches, which form the terminal processes of the candelabrum.

When quantifying the branching pattern of the PVD in adulthood, WT (or WT-like *him*-5 background) animals which were isolated as embryos showed an increase in ectopic branching compared with crowded age-matched worms (Fig. 2B) and the quaternary branches assumed a more rippled shape (fewer straight 4ry branches, Fig. 2C), regardless of the neuron marker utilized (see Fig. S2).

To determine whether chemical stimulation plays a role in the observed morphological plasticity, animals were isolated onto pheromone-conditioned plates (Maures, Booth et al., 2014). Similarly to the response to harsh touch (Fig. 1D), chemical stimulation of the plates did not rescue the isolation-induced increase in the fraction of ectopic branching or the decrease in percentage of straight quaternary branches (Fig. S3). Additionally, we looked at *mec-4* gentle-touch-insensitive mutants (Rose et al., 2005, Suzuki et al., 2003) and found that isolation caused a similar change to PVD structure as in the WT (Fig. S4, compare with Fig. 2B and 2C). In summary, these results suggest that mechanosensory experience controls morphological plasticity of PVD dendritic trees independently of *mec-4* and chemical stimulation.

We next sought to determine whether DEG/ENaCs mediate these experience-driven morphological alterations, by examining PVD morphology in crowded and isolated *mec-10* mutants. We found that crowded *mec-10* animals were different from WT crowded worms, and appear more isolated-like in terms of morphological features (more ectopic branches and fewer straight quaternary branches, compared to crowded *him-5* control animals; Fig. 2B and 2C). These results suggest that PVD dendritic morphology is affected by sensory experience in a *mec-10*-dependent pathway. Importantly, these results confirm a role for the mechanosensory channel MEC-10, but not other degenerins (such as ASIC-1), in the plasticity of both the dendritic structure and the nociceptive function of the PVD in the crowded background.

To study whether *mec-10* acts cell autonomously to mediate morphological plasticity, we again utilized PVD-specific MEC-10 expression in a *mec-10* mutant background and found it reduced the fraction of ectopic branches and increased the percentage of straight quaternary branches, compared to age-matched crowded *mec-10* animals without the rescue array (Fig. 2D-I). Thus, MEC-10 acts in the PVD to mediate morphological plasticity.

Having identified an isolation-induced morphological plasticity in adults (observed at 72 h from embryo), we next sought to establish the temporal dependence of the effect, by comparing animals after only 48 h, as young adults (see Fig. S5A). Isolated worms showed a small but significant difference for the percentage of straight quaternary branches, but not in ectopic branching (Fig. S5B-E) when compared with age-matched crowded worms, suggesting that isolation induces some morphological alterations during morphogenesis, while some relate to adult-stage maintenance of the neuron. We then isolated animals grown for 48 h in crowded conditions, and found that isolation of young crowded adults for 24 h induced changes in both measured

247 parameters (Fig. S5F-I), recapitulating isolation of embryos (Fig. 2B-C). Thus, isolation
248 of adults for 24 h is sufficient to affect PVD dendritic tree architecture, in contrast to the
249 developmentally-established behavioral response (Fig. 1G).

250 To further determine whether the morphological effect on PVD structure is solely
251 mediated by mechanical cues, we used glass beads under isolated conditions. We
252 found that while the presence of glass beads did not reduce the fraction of ectopic
253 branching, it significantly increased the number of straight quaternary branches
254 (compared with isolated animals without beads, Fig. 2J-K). Thus, the mechanosensory
255 stimuli of inert beads can partially rescue isolation-induced morphological changes to
256 the PVD.

257 **Isolation triggers dynamic plasticity of the dendritic tree**

258 To pinpoint the precise time interval required to mediate dendritic arborization changes
259 in adulthood, we examined the effect of varying isolation times on the PVD morphology
260 of crowded-raised young adults. We found that isolation of adults for 2 h had no
261 significant consequence on the structure of the PVD, while isolation of adults for 5 h or
262 longer, significantly increased the proportion of ectopic branches and reduced the
263 percentage of quaternary straight branches compared to crowded worms (Fig. 3A-B).

264 To further study plasticity at the individual level, we compared the dendritic tree
265 of individual worms grown under crowded conditions before and after 4 h isolation. This
266 revealed isolation induced more events of ectopic branch growth and fewer events of
267 branch retraction (Fig. 3C). Furthermore, this period was sufficient to induce an increase
268 in ectopic branching and a decrease in percentage of straight quaternary branches
269 (Figs. 3D, 3E, and S6). Thus, 4 h of isolation are sufficient to induce changes in the
270 architecture of the adult PVD.

271 Since the geometry of quaternary branches shows rapid response to the amount
272 of mechanosensory stimulation (Fig. 3A-E), we next asked how dynamic is this
273 experience-dependent morphological change. We performed a 3 h time lapse imaging
274 in crowded and isolated animals anesthetized with 1% tricaine (Movies S1 and S2). We
275 found that while the number of straight quaternary branches in the isolated worms
276 remained low and stable (~8%), for the crowded animals, we observed a gradual
277 reduction in straight quaternary branches, starting after ~2 h of isolation of individual
278 worms on the slide (Fig. 3F,G).

279 In summary, isolation-induced morphological plasticity is apparent within 2-3 h
280 from the switch from crowded conditions to growth in the absence of mechanical stimuli.
281 This dynamic process involves simultaneous increase in ectopic branching and
282 decrease in straight terminal branches.

283 **Activity affects morphology**

284 It has been shown that activity and sodium influx via the DEG/ENaC UNC-8 promotes
285 synapse elimination in *C. elegans* (Miller-Fleming, Petersen et al., 2016). To test how
286 global inhibition of DEG/ENaCs affects the morphology of the PVD neuron, we
287 evaluated crowded worms that were grown on plates with amiloride compared to control
288 worms. We found that blocking DEG/ENaCs by amiloride increased the fraction of
289 ectopic branching and decreased the percentage of straight quaternary branches (Fig.
290 S7A-D). Thus, unlike harsh touch response, which is independent of sensory-level
291 global inhibition (Fig. S1C), global inhibition at the sensory level alters dendritic
292 morphology. These results suggest that activity via degenerins modulates the structure
293 of the PVD.

294 To test whether manipulations of other neuromodulators can affect the branching
295 dynamics of the PVD, we utilized two anesthetics: tetramisole, which activates the
296 nematode nicotinic acetylcholine receptors inducing muscle contraction (Aceves, Erlij et
297 al., 1970) and tricaine, which modulates neuronal activity by blocking sodium channels
298 (Katz, Chu et al., 2020) and analyzed their effects during 2-3 h of time lapse movies of
299 crowded and isolated animals. We first tested the commonly used mixture of 0.1%
300 tricaine and 0.01% tetramisole (the racemic mixture of the enantiomer levamisole)
301 (Kravtsov et al., 2017) and found that it induces more growth than retraction of ectopic
302 branches in crowded animals (Fig. S7E-G). In contrast, 1% tricaine alone has the
303 opposite effect- more retractions of ectopic branches (Fig. S7H-I; Movies S1 and S2). In
304 addition, 1% tricaine induces more growth for isolated compared to crowded worms,
305 indicating that there are activity-dependent intrinsic factors that are different for the two
306 experience states. These results suggest that modulating neuronal activity triggers
307 structural modifications in the PVD, indicating a possible structural sensitivity to the
308 amount of neuronal activity. In summary, we found that mechanosensory experience,
309 DEG/ENaC protein presence and activity, and pharmacological targeting of activity
310 dynamically affect the structure of the PVD.

311 **PVD structure and function are independent**

312 After establishing that mechanosensory experience induces both a behavioral and a
313 structural plasticity of the PVD, we asked whether there is a causal link between the
314 morphology of the dendritic tree of the PVD and its function as a nociceptor (Hall &
315 Treinin, 2011). We followed the isolation protocol described in Fig. 1B for seven
316 combinations of DEG/ENaC mutants and analyzed their response to harsh touch (Fig.
317 S8) and their PVD structure (Fig. S9). In order to compare the morphological properties
318 of the different DEG/ENaC genotypes under different sensory experience (crowded,
319 isolated; Fig. S9), we used discriminant analysis. This provides a supervised
320 classification method to combine all the analyzed morphological phenotypes, including
321 loss of self-avoidance between adjacent candelabra (Fig S10), into a certain value
322 characterizing the PVD morphological state (Fig. 4A). We then superimposed the
323 behavioral results of the DEG/ENaC mutants' response to harsh touch (Fig. S8) on the

morphological clustering, as a binary-like property (<45% responding for isolated WT versus >65% for crowded WT, as shown in Fig. S8*)*. We found no correlation between the morphology of the PVD and the response to harsh touch when testing the different combinations of genotypes and treatments. For example, isolated *mec-10;degt-1* double mutants show crowded-like morphology with isolated-like behavioral response (Fig. 4A and Fig. S8, S9). These findings suggest that while degenerins are required for isolation-induced plasticity of both traits, response to harsh touch is independent of the structural alteration of the PVD.

An additional line of evidence supporting the independence of the behavioral and morphological phenotypes was demonstrated by isolation of young adult worms for 24 h (Fig. 3). This isolation affects the structure of the PVD (Fig. S5) but has no effect on the response to harsh touch (Fig. 1G). Amiloride also has no effect on harsh touch response (Fig. S1C) but does alter dendritic morphology (Fig S7 A-D). Finally, to directly demonstrate that these two features are independent, we assayed harsh touch responses of isolated animals and then analyzed each individual animal for its PVD morphology. We then compared the dendritic morphology of responding and non-responding worms, and found that the morphological parameters were similar (Fig. 4B-E). Thus, analysis at the level of individual worms failed to demonstrate a correlation between the morphology and the response to harsh touch. In summary, the morphological and behavioral phenotypes were independently affected by sensory experience via degenerins. We cannot exclude the possibility that other functions of the PVD, like the response to low temperatures (Chatzigeorgiou et al., 2010) and proprioception (Albeg et al., 2011) are more tightly associated to the structure of the PVD, nor that the morphological changes induced by isolation are too minor to constitute a difference in neuronal function.

In addition to the isolation-induced changes in the number of ectopic branches and the percentage of straight quaternary branches, we found that worms raised in isolation are also more likely to lose the self-avoidance between two adjacent menorahs (candelabra). This effect is also *mec-10*-dependent, but appears to act cell non-autonomously. In addition, it is chemosensory and amiloride independent (Fig. S10).

MEC-10 and DEGT-1 localization is experience-dependent

Differential localization of degenerins can affect both the behavioral response to harsh touch and the structural properties of the neuron. When considering the effect of isolation, we hypothesized that changes in the localization patterns of DEG/ENaC can account for plasticity at both the behavioral (Fig. 1) and the structural level (Figs. 2, 3). Since MEC-10 and DEGT-1 tend to co-localize within the PVD (Chatzigeorgiou et al., 2010) we analyzed the interaction between these two proteins, under different mechanosensory experiences. We found that MEC-10 localization in the plasma membrane, in intracellular vesicular compartments of the axon and in the quaternary branches was reduced after isolation (Fig. 5A-D, Movies S3 and S4). In contrast to

364 MEC-10 (Figs. 5A-D), DEGT-1 localization is reduced only in the cell body following
365 isolation (Fig. 5E-H). Furthermore, *degt-1* mutants reduced the overall amount of MEC-
366 10, and more importantly, abrogated the isolation-induced reduction in MEC-10
367 localization at the quaternary branches and the axon (Fig. 5A-D). In the reciprocal
368 experiment, DEGT-1 localization was affected in *mec-10* mutants, as isolated worms
369 exhibit increased localization to the cell body compared with WT isolated worms (Fig.
370 5E-H). Thus, mechanosensory experience also induces plasticity in the localization
371 pattern of MEC-10 and DEGT-1. We propose this differential localization may be part of
372 the mechanism that independently and locally modulates dendritic and axonal
373 properties, to affect both the structure and the function of the PVD, respectively.

374 **Optogenetic stimulation suggests behavioral plasticity is post-sensory**

375 We have shown that sensory deprivation (isolation) affects the localization of two
376 different mechanoreceptors, the degenerins MEC-10 and DEGT-1 in the dendrites,
377 axon and soma of the PVD. It is conceivable that the differential localization of
378 degenerins in different domains of the PVD may affect the morphology and function of
379 the PVD. Thus, we decided to stimulate the PVD independently of the endogenous
380 mechanoreceptors and study whether the escape behavior following harsh touch is
381 similar in isolated and crowded animals. We hypothesized that if we circumvent the
382 normal degenerin-mediated mechano-stimulation, exciting the PVD downstream to
383 sensory activity, the animals grown in isolation will respond to the same degree as if
384 they were in crowded conditions and independently of the dendritic tree morphology.
385 Optogenetic stimulation is an elegant way to bypass the sensory perception mediated
386 by receptors and transduced by diverse signal transduction pathways (Husson et al.,
387 2012). Thus, to investigate whether the isolation-induced decreased response to harsh
388 touch is a PVD-dependent function, we used optogenetic stimulation with
389 Channelrhodopsin (ChR2) expressed in the PVD (Husson et al., 2012). We found that
390 isolation significantly reduced the percentage of worms responding to optogenetic
391 stimulation of the PVD (Fig. 5I), indicating that the plasticity in the response is acting
392 downstream to PVD activation, mechanosensory channels and signal transduction
393 pathways. This activation is sensitive to isolation probably because it is acting pre- or
394 post-synaptically. To determine whether optogenetic stimulation of isolated animals can
395 reverse the morphological changes induced by the absence of mechanical stimuli in
396 PVD, we used optogenetic stimulation of the PVD and found no significant difference
397 between isolated and isolated-optogenetically-stimulated animals in terms of any
398 measured PVD structural characteristic (Fig. S11). Thus, optogenetic stimulation on
399 isolated animals is not sufficient to convert their dendritic trees to crowded-like. In
400 addition, isolated animals respond to optogenetic stimulation in a reduced way
401 suggesting that the escape response is not dependent on the structure of dendritic trees
402 but on unknown downstream pathways.

403 In summary, genetic, and pharmacological evidence suggest that dendritic structural
404 plasticity is an autonomous activity-dependent homeostatic mechanism. Combined with
405 optogenetic testing, our results indicate the mechanosensory dendritic tree morphology
406 is independent from pre- or post-synaptic degenerin-mediated processes that affect
407 behavioral escape in response to harsh touch.

408 **Discussion**

409 From the evolutionary point of view, dendritic trees and their structural complexity
410 remain mysterious objects, despite many efforts to understand the contribution of
411 arborization complexity to dendritic physiology and function (Hausser & Mel, 2003).

412 Previous research has demonstrated both cell autonomous (Aguirre-Chen, Bulow
413 et al., 2011, Oren-Suissa et al., 2010, Salzberg et al., 2014) and cell non-autonomous
414 (Dong et al., 2013, Salzberg et al., 2013) mechanisms that regulate the PVD's dendritic
415 morphogenesis during development. Some studies have also focused on regeneration
416 and aging effects on the tree structure of the PVD, revealing plasticity in the adult stage
417 (Iosilevskii & Podbilewicz, 2021, Kravtsov et al., 2017, Oren-Suissa et al., 2017), similar
418 to what has been shown for Drosophila sensory neurons (DeVault, Li et al., 2018). We
419 found, by using mutants for degenerins, chemosensory stimulation controls,
420 pharmacology, optogenetics and glass beads, that the dendritic structure of the PVD
421 and the behavioral response to harsh touch are activity- and mechanosensory-
422 dependent, but appear to be chemosensory-independent. It is still conceivable that
423 chemosensation can affect nociception and proprioception, in some sort of a cross
424 modal plasticity mechanism, but at the moment we do not have evidence for this
425 scenario in the PVD, where we show that mechanosensory channels (DEG/ENaCs)
426 affect the architecture of the PVD.

427 Our results suggest that 'nurture', manifested as mechanosensory experience,
428 activates mechanotransduction signaling, via DEG/ENaCs amiloride-sensitive activity,
429 to stabilize the homeostatic structure of the dendritic tree in adults. The sensory
430 experience induced when one body side of the worm is in contact with the agar plate is
431 not sufficient for this purpose (Fig. S12); however, other worms on the plate, or the
432 presence of glass beads, elicit significant structural alterations. Moreover, the cell
433 autonomous activity of MEC-10 in the PVD was found to be both necessary and
434 sufficient to preserve the crowded-experience phenotype in terms of the simplified
435 structure of the PVD. While there are other multiple plausible explanations, our failure in
436 remodeling the isolated-state arbor by repeated optogenetic activation of the PVD may
437 provide further evidence for the necessity of degenerins in this structural plasticity, since
438 neuron activation by ChR2 bypasses the activation of mechanically-gated degenerin
439 channels. Figure 6 depicts our working model, where the amount of mechanosensory
440 stimulation, in crowded or isolated conditions, affects the expression and localization of
441 MEC-10 and DEGT-1 in different compartments of the PVD. Localization of MEC-10,
442 probably by forming higher-order complexes with other DEG/ENaCs, can affect the

structure of the PVD at the level of the dendritic tree. The morphological and behavioral phenotypes shown here were rescued by a PVD-specific expression of MEC-10, supporting such a cell autonomous mechanism. The experience-induced structural plasticity seems homeostatic at the individual branch dynamics level in the adult. In contrast, we show that the behavioral response to harsh touch is modulated by mechanosensory experience during development and by the presence of degenerins, and perhaps involves other neurons downstream. Based on optogenetic stimulation, we presume that the behavioral plasticity is a pre- and/or post-synaptic property, mediated by DEG/ENaC (Hill & Ben-Shahar, 2018) and related to neurotransmission modulation, independently of the structure of the PVD dendritic tree. These structural and behavioral plasticity are separated in time (adulthood vs. development) and space (dendrite vs. axon; Fig. 6). We found no correlation or causation between the structure and the nociceptive function of the PVD. It is possible that such a link exists, but our physiological and behavioral outputs are not sensitive enough to detect it.

Somatosensory activation in vertebrates plays a prominent role in shaping the structural and functional properties of dendritic spines, mainly studied in the central nervous system (Gyorffy, Kun et al., 2018, Holtmaat & Svoboda, 2009, Xu, Yu et al., 2009, Yang, Pan et al., 2009). In contrast to mammalian cortical neurons, much less is known about sensory neurons' degree of plasticity and the molecular mechanisms utilized during adulthood. Here we suggest that degenerins mediate mechanosensation-induced dendritic growth in sensory dendrites. The dendritic plasticity we described bears resemblance to the activity-dependent effect of glutamatergic signaling and NMDA receptors. Activity via NMDA affects dendritic spines as an upstream mechanism of cell signaling, resulting in structural modifications (Nagerl, Eberhorn et al., 2004, Star, Kwiatkowski et al., 2002, Stein, Park et al., 2021, Zhang, Cudmore et al., 2015). It is possible that degenerins mediate mechanosensory signaling sensation, by activating cationic gradients (Kellenberger & Schild, 2002), leading to activation of downstream intracellular signaling pathways (Ghiretti et al., 2014, Sin et al., 2002, Vaillant et al., 2002, Zhou et al., 2006), which in turn stabilize local, actin-mediated (Halpain, 2018, Luo, 2002, Zuo et al., 2005) structural plasticity in the PVD dendritic branches. In *Drosophila,* at the epithelium, mechanosensitive ion channels, together with E-cadherin-catenin complexes and calcium sensing mechanisms affect epithelial morphogenesis (Roy Choudhury, Groflhans et al., 2021). In parallel, DEG/ENaCs may also modulate pre- and post-synaptic homeostatic signaling in the harsh touch circuit, as has been shown in neuromuscular junctions (Younger, Muller et al., 2013). While this study focuses on degenerins activation in the PVD with emphasis on dendritic structures, future studies may establish the pre- and -post-synaptic mechanisms which act downstream, on the transcriptional and translational levels. These directions for future studies have the potential to increase our understanding of the mechanisms that couple sensory experience, to structural dendritic plasticity.

483 In summary, we propose that the combinatorial actions of DEG/ENaCs have
484 mechano-signaling functions mediating plasticity in sensory dendritic trees, and provide
485 mechanistic insights into dendritic structural responses to sensory experience in
486 adulthood and the behavioral consequences of such adaptations during development.
487

488 **Materials and Methods**

489 **Strains**
490 Nematode strains were maintained according to standard protocols (Brenner, 1974).
491 The list of the strains is presented in Supplementary Table 1. Strains of the DEG/ENaCs
492 family obtained from the CGC (JPS282: *asic-1*(*ok415*) I; ZB2551: *mec-10*(*tm1552*) X;
493 VC2633: *degt-1*(*ok3307*) V) were crossed with BP709: *hmnIs133[ser-2Prom3::kaede]*.
494 The validation of F2 homozygotes for the DEG/ENaCs deletions (including single,
495 double and triple mutants) was performed by PCR amplification of the genomic area
496 containing the deleted region.

497 Primers for Multiplex PCR

498 The list of the primers used is presented in Supplementary Table 2.

499 **Spinning disk confocal microscopy**
500 Prior to imaging, the worms were mounted on a 10% agar pad placed on a microscope
501 glass slide, in 1µl polystyrene beads (100 nm diameter; Polysciences, Inc.) for their
502 mechanical restraint, and sealed with a coverslip for complete physical immobilization
503 (Kim, Sun et al., 2013). The PVD neuron was visualized using a Yokagawa CSU-X1
504 spinning disk, Nikon eclipse Ti inverted microscope and iXon3 camera (ANDOR).
505 Images were captured with MetaMorph, version 7.8.1.0. For each worm, a sequential z-
506 series image stack (step size of 0.35 µm) was obtained with an oil Plan Fluor 40X (NA
507 1.3) lens around the PVD cell body, encompassing approximately 50-100 µm segments
508 both anteriorly and posteriorly.

509 **Data analysis**
510 The analysis of the PVD structure was performed for the area surrounding the cell body.
511 All images were analysed with ImageJ, version 1.48 (NIH), in TIFF format, by producing
512 a maximal intensity z-series projection and converting it to negative form (invert lookup
513 table) for improved visibility. Ectopic branching was defined as described previously
514 (Hausser & Mel, 2003). Briefly, non-ectopic branches form the 'ideal' WT candelabrum
515 of the late L4 stage, whereas excess branches, which create non-quaternary terminal
516 ends, are considered ectopic, as illustrated with dashed lines for ectopic branching in
517 Fig. 2A. The total number of ectopic and non-ectopic branches was quantified for each
518 image, and presented as a fraction (ectopic/non-ectopic branches).
519 The geometry of each quaternary branch ("candle") was defined in the following
520 manner: Straight geometry- all the pixels that constitute the branch are positioned on a

521 straight line generated with ImageJ. The width of the line (1 pixel) was constant for the
522 entire sets of experiments. The number of straight quaternary branches were divided by
523 the total quaternary branches in the image for each worm and presented as a
524 percentage. The analysis was done only for worms which did not move through the Z
525 series. Moving worms were excluded from the experiment. Self-avoidance defects- the
526 number of events where two adjacent candelabra overlapped (no gap formation), was
527 divided by the total number of gaps between the candelabra within the frame (Fig. 2A).
528 The self-avoidance values are presented as percentage.

529 **Behavioral procedures**

530 **Harsh touch assay**
531 After 72 h, adult worms (both isolated and those from the crowded plate as described
532 below) were transferred using an eyelash each to a new agar plate, freshly seeded with
533 150 µl OP50 (about 16 h after seeding). This step is required to avoid a thick edge of
534 the bacterial lawn, which might interfere with harsh touch response measurement. After
535 ~45 minutes in the plate, the non-moving worms were prodded with a platinum wire
536 posterior to the vulva, above the interface between worm's body and the agar plate
537 (Way & Chalfie, 1988), every 10 seconds, and the number of responses to harsh touch
538 was counted. Animals with a functional PVD moved, sometimes backing up. More than
539 one response constitutes a responsive animal. The non-responding worms were
540 defined if two prodding events were observed sequentially without response. The
541 percentage of responding worms was calculated for each genotype and treatment. The
542 experimenter was blind to both the genotype and the treatment- crowded or isolated.

543 **Isolation of embryos**
544 To establish the method for conspecifics based mechanosensory stimulation, we
545 performed several calibration experiments with different population densities (250
546 embryos, 15 adults, 30 adults) to test conditions for the crowded plate.
547 We found a gradual increase in the crowding effect and reduced variation in the
548 measured parameter. Following that, we decided to work with the group of 30 crowded
549 adults" as a source of mechanosensory signal.
550
551 The worm isolation procedure was based on previous work (Rose et al., 2005) with a
552 few modifications, as indicated. Isolated animals were grown on 6 cm agar plate with
553 150 µl of OP50 *E. coli*, while crowded plate worms were grown on 600-700 µl OP50 to
554 prevent starvation. The embryos and adult worms were isolated with platinum wire. The
555 plates were sealed with one layer of Parafilm M and placed into a plastic box, at 20 ºC,
556 for the entire experiment.
557 Three experimental groups were used for the 72 h (96 h of experiment was performed
558 only for *mec-4* worms, since they were L4- very young adults at 72 h) isolation
559 experiment: **(1)** Single isolated embryos **(2)** Crowded worms - the progeny of 30 young,
560 non-starved, adults (approximately, 7,000-9,000 worms in different developmental

561 stages, without approaching starvation) **(3)** Crowded adult worms that were isolated for
562 a certain amount of time as adults.
563 After 48/72/96 h (according to the experiment), age-matched worms from each group
564 were transferred to 10% agar pad slides for imaging, as described above (Rose et al.,
565 2005).

566 **Isolation of adults for 2, 5, 15 or 24 hours**
567 Crowded plates were prepared as described above, with progeny from 30 adult
568 hermaphrodites. Animals were separated into individual plates for the desired time
569 window before 72 h have passed (*i.e.* after ~70 h for 2 h isolation, ~67 h for 5 h isolation
570 etc.). Worms were isolated using an eyelash into new plates containing 150 µl of OP50.
571 At 72 h, the PVD of isolated animals was imaged and compared with age-matched
572 animals which remained in the crowded plate of origin (see Fig. 1B).

573 **Optogenetics stimulation for harsh touch**
574 Crowded and isolated worms (ZX819: *lite-1(ce314) X;*
575 *xIs12[pF49H12.4::ChR2::mCherry; pF49H12.4::GFP*]) were grown on OP50 with 100
576 µM All Trans Retinal (ATR, Sigma R2500), in order to obtain functional
577 Channelrhodopsin (Husson et al., 2012) (as a control we tested the response of worms
578 that were grown on ethanol alone, no response was detected for these worms). After 72
579 h the worms were singly mounted with eyelash on a chunk (1cm X 1cm) of agar that
580 was mounted on a microscope glass slide. The agar contained fresh but dry OP50, with
581 100 µM ATR. About 30 minutes following the transfer the worms were tested for the
582 response to light. Worms were stimulated at 488 nm wavelength, with laser intensity of
583 40% and exposure time of 100 ms, with 10X Plan Fluor (NA 0.3) for ~1 second and the
584 forward acceleration response was measured. The microscope system is as described
585 above. The experimenter determined the presence or the absence of forward
586 acceleration in response to light activation.

587 **Optogenetics stimulation of isolated worms**
588 Isolated eggs were grown as described at the 'Isolation of embryos' section.
589 Isolated worms (ZX819: *lite-1(ce314) X; xIs12[pF49H12.4::ChR2::mCherry;*
590 *pF49H12.4::GFP*]) were grown on 150 µM OP50 with 100 µM ATR (Husson et al.,
591 2012) or 0.3% ethanol as control. After 72 h both the crowded and isolated worms were
592 singly mounted with eyelash onto a cube (with surface area of about approx.1cm^2,
593 depth of 0.5 cm) of agar layered with fresh, fully dried, OP50 with 100 µM ATR or 0.3%
594 ethanol as a control group. The worms were stimulated with 488 nm wavelength, with
595 laser intensity of 40% and exposure time of 100 ms, with 10X Plan Fluor (NA 0.3) for
596 ~60 seconds, every 5 min during 4 h. Stimulation and recording was performed with the
597 microscope system described above.
598 As a control, before each experiment, crowded ZX819 worms were tested for forward
599 acceleration as a positive control to the functionality of the ChR2. After the end of 4 h

600 stimulation, the worms were mounted for imaging of the PVD at 40X as described under
601 "Spinning disk confocal microscopy" section.

602 **Isolation with chemical stimulation**

603 The *glp-4(bn2)* mutants which are sterile at 25 °C were used (~40 worms for each
604 plate), in order to prepare conditioned/chemically stimulated plates (Maures et al., 2014)
605 prior to growing isolated animals. The *glp-4* mutants were transferred at early larval
606 stage (L1, L2) to a new agar plate for 96 h at 25 °C. After the removal of the *glp-4*
607 mutants, the embryo isolation procedure was used, as described before at 20 °C.

608 **Isolation with glass beads**

609 Single embryos were isolated to agar plates with 150 µl OP50 and 2.5 g of glass beads
610 (1 mm diameter) were placed on the OP50 lawn in the middle of the plate. The worms
611 were isolated for 72 h and tested for response to harsh touch as described above.

612 **Pharmacology**

613 Amiloride hydrochloride hydrate (Sigma, #A7410) 1 M stock solution in DMSO was
614 stored at -20°C. A final concentration of 3 mM amiloride in 0.03 % DMSO was prepared
615 in OP50 bacteria (LB medium) and seeded on NGM plates. 650 µl of the OP50 mixture
616 was seeded on each plate. As a control, 0.03 % DMSO was added to OP50 bacteria.
617 For each plate (control 0.03% DMSO or 3 mM amiloride) 30 non-starved adult worms
618 were added. After 72 h at 20 °C the progeny of the 30 adults were tested as young
619 adults for their PVD morphology and their response to posterior harsh touch, as
620 described in the previous sections.

621 **Anesthetics and long-term imaging**

622 In addition to immobilization of worms with 100 nm polystyrene beads as described in
623 the "Spinning disk confocal microscopy" section above, two additional methods for long
624 term imaging and pharmacological effects assays were used: 1% tricaine (Sigma,
625 A5040) in M9 buffer or a mixture of 0.01% tetramisole (Sigma, T-1512) and 0.1%
626 tricaine in M9 buffer were utilized.
627 Worms were exposed to the anesthetics (in a glass well) for ~20 min until paralyzed,
628 then transferred to 3% agar pads with 1 µl of the anesthetics. Sequential z-axis image
629 series (0.6 µm step-size) were taken, as described above, every 5 min for 2-3 h.

630 **Imaging individual worms- crowded to isolated**

631 Worms were grown at crowded conditions, as described above. At ~24 h of adulthood,
632 individual worms were placed in a 1% tricaine solution in M9 buffer for 10 min until
633 paralyzed and transferred to 3% agar slides with 1 µl 1% tricaine. Following a short
634 PVD imaging session, the worms were recovered from the slide with M9 and isolated to
635 a new plate for 4 h. Each 4 h-isolated animal was anesthetized once again with 1%
636 tricaine for 10 min prior to PVD imaging.

637 **Analysis of DEG/ENaCs localization in the PVD**

638 Two DEG/ENaCs protein constructs, pF49H12.4::MEC-10::mCherry and
639 pF49H12.4::DEGT-1::mCherry (plasmids kindly provided by W. Schafer's lab,
640 (Chatzigeorgiou et al., 2010)) were analysed for their localization in the PVD, by
641 comparing worms expressing the co-injection marker *punc-122*::GFP raised in crowded
642 or isolated conditions, in a similar behavioral assay as described in Fig. 1B. A z-series
643 (step size of 0.35 µm, immobilization performed with polystyrene beads, as described in
644 the microscopy section) of the area around the cell body of the PVD was obtained with
645 a 60X Apochromat (NA 1.4) lens. The images (after maximal intensity projection of the
646 Z-series) were encoded so the analysis was performed in a blind manner. The presence
647 or absence of fluorescent signal was examined in three compartments: The cell body,
648 the quaternary branches and the axon of the PVD.

649 **Rescue strains**

650 Worms from BP1022 (*mec-10(tm1552)* X; *hmnIs133[ser-2Prom3::Kaede]*; *him-5(e1490)*
651 V) were injected into the gonad with a rescuing plasmid for *mec-10*, with a PVD specific
652 promoter (pWRS825: *ser-2Prom3::mec-10* genomic) kindly provided by W. Schafer's
653 lab (Chatzigeorgiou et al., 2010). The injection mix contained *myo-2p::GFP* (20 ng/µl) as
654 a co-transformation marker and pWRS825 (80 ng/µl). For both behavioral and structural
655 characterization, the *him-5;mec-10* strains, with and without rescuing plasmid, shared
656 the same crowded plate and were differentiated by the presence or absence of the co-
657 injection marker.

658 **Effect of plate on PVD in contact with agar and the opposing side**

659 Embryos were singled into plates with 150 µl OP50 bacteria at 20°C, and
660 analyzed as young adults 72 h later. Every animal was transferred using an
661 eyelash into freshly seeded plates (<24 h), and noted for its side orientation.
662 Once on these experiment plates, animals were observed for their side
663 orientation at 30-minute intervals for a minimum of 3 h prior to microscopy.
664 For microscopy of both PVD neurites, while few animals were removed from the slide
665 and repositioned using an eyelash, most animals were imaged using a coverslip
666 'sandwich' method (adapted from (Sulston, Schierenberg et al., 1983)), whereby the
667 animal is pressed on an agar pad between two large coverslips, which are subsequently
668 flipped as a single unit and observed from the other side. Briefly, a thin 3% agar pad
669 was pressed onto a 24x50 mm coverslip (170±5 µm thick), placed on a standard
670 microscope slide for ease of handling. Animals were singly placed in a drop of 0.05%
671 tetramisole (Sigma, T-1512) in M9 on the agar pad using an eyelash, and a second,
672 similar coverslip was immediately placed above. The two coverslips were sealed shut
673 onto the supporting slide using two thin strips of marking tape, and once the animal was
674 anaesthetized the PVD on the side closest to the objective was imaged as described
675 above (see Spinning Disk confocal microscopy). For viewing the opposite neurite, the
676 tape was carefully peeled and the two coverslips flipped as one, taped again, and
677 similarly imaged. Note that this method inevitably makes the second side imaged to be
678 fainter due to the laser penetrating through the agar pad layer itself; laser intensities

were typically increased by up to 5% in order to compensate for the decrease in fluorescence.

Statistics and data plotting

At least two independent experiments constitute the data set described in each figure. For the morphological characterization of the PVD the results are expressed as means (blue circle) ± standard error of the mean (s.e.m.). In the boxplot (first, third quartiles) the upper whisker extends from the hinge to the highest value that is within 1.5 * IQR (inter-quartile range), the distance between the first and third quartiles. The lower whisker extends from the hinge to the lowest value within 1.5 * IQR of the hinge.
The statistical analyses were performed with SPSS software (IBM, version 20) and "R package". Two-tailed tests were performed for the entire data sets.
Since for many experiments the distribution of the data was not normal, nonparametric tests were used: Mann-Whitney test for comparison between two independent groups. Kruskal-Wallis test was used for multiple comparisons for more than two groups.
For proportions (percentage worms) ± standard error of proportion was calculated. Fisher's exact test was used for analysis of differences in proportions. To estimate the variability in proportion we calculated the Standard Error of Proportion: $\sqrt{\frac{(1-p)\cdot p}{n}}$
The dot plot figures were prepared with "R package", the bar charts with Microsoft Excel software. Final figures were prepared with Adobe Illustrator CS version 11.0.0.

Discriminant analysis

Eight different strains (WT and seven DEG/ENaCs), with two treatments (crowded, isolated worms) for each strain were analyzed for Linear discriminant analysis for morphological characteristics, to evaluate similarity between different strains and treatments. Each worm in the data set was characterized by the three morphological characteristics (the fraction of ectopic branching, the percentage straight quaternary branches and the percentage of self-avoidance defects). The centroid for morphological characterization was calculated for each condition and represented by a square. Data from independent harsh touch experiments are shown for each group. The analysis was performed using SPSS 20.

Acknowledgments

We thank current and former lab members for their intellectual and technical support. Veronika Kravtsov, Sagi Levy, Anna Meledin, Meital Oren-Suissa, Tom Shemesh, Shay Stern, Yehuda Salzberg and Alon Zaslaver for critically reading and commenting on the manuscript. Ehud Ahissar, Dan Cassel, Michel Labouesse and Kang Shen for fruitful discussions. William Schafer, Max Heiman, Hannes Bulow, Yehuda Salzberg and Alexander Gottschalk for plasmids and strains. Some strains were provided by the Caenorhabditis Genetics Center (CGC), which is funded by NIH Office of Research Infrastructure Programs (P40 OD010440). This work was supported by grants from the Israel Science Foundation (442/12 and 257/17), Adelis Fund (2023479), and the Ministry of Science and Technology (3-13022).

References

Aceves J, Erlij D, Martinez-Maranon R (1970) The mechanism of the paralysing action of tetramisole on Ascaris somatic muscle. British journal of pharmacology 38: 602-607

Aguirre-Chen C, Bulow HE, Kaprielian Z (2011) C. elegans bicd-1, homolog of the Drosophila dynein accessory factor Bicaudal D, regulates the branching of PVD sensory neuron dendrites. Development 138: 507-18

Albeg A, Smith C, Chatzigeorgiou M, Feitelson DG, Hall DH, Schafer WR, Miller DM, 3rd, Treinin M (2011) C. elegans multi-dendritic sensory neurons: Morphology and function. Mol Cell Neurosci 46: 308-317

Alvarez VA, Sabatini BL (2007) Anatomical and physiological plasticity of dendritic spines. Annual review of neuroscience 30: 79-97

Bailey NW, Moore AJ (2018) Evolutionary Consequences of Social Isolation. Trends in ecology & evolution 33: 595-607

Baldin JP, Barth D, Fronius M (2020) Epithelial Na+ Channel (ENaC) Formed by One or Two Subunits Forms Functional Channels That Respond to Shear Force. Frontiers in Physiology 11

Ben-Shahar Y (2011) Sensory Functions for Degenerin/Epithelial Sodium Channels (DEG/ENaC). Adv Genet 76: 1-26

Bianchi L, Driscoll M (2002) Protons at the gate: DEG/ENaC ion channels help us feel and remember. Neuron 34: 337-340

Brenner S (1974) The genetics of *Caenorhabditis elegans*. Genetics 77: 71-94

Caneo M, Julian V, Byrne AB, Alkema MJ, Calixto A (2019) Diapause induces functional axonal regeneration after necrotic insult in C. elegans. PLoS Genet 15: e1007863

Chalfie M, Sulston J (1981) Developmental genetics of the mechanosensory neurons of Caenorhabditis elegans. Dev Biol 82: 358-370

Chatzigeorgiou M, Yoo S, Watson JD, Lee WH, Spencer WC, Kindt KS, Hwang SW, Miller DM, 3rd, Treinin M, Driscoll M, Schafer WR (2010) Specific roles for DEG/ENaC and TRP channels in touch and thermosensation in C. elegans nociceptors. Nature neuroscience 13: 861-868

Chen Y, Bharill S, Isacoff EY, Chalfie M (2015) Subunit composition of a DEG/ENaC mechanosensory channel of Caenorhabditis elegans. Proc Natl Acad Sci U S A 112: 11690-11695

Collet J, Spike CA, Lundquist EA, Shaw JE, Herman RK (1998) Analysis of osm-6, a gene that affects sensory cilium structure and sensory neuron function in Caenorhabditis elegans. Genetics 148: 187-200

DeVault L, Li T, Izabel S, Thompson-Peer KL, Jan LY, Jan YN (2018) Dendrite regeneration of adult Drosophila sensory neurons diminishes with aging and is inhibited by epidermal-derived matrix metalloproteinase. Genes Dev 32: 402-414

Dong X, Liu OW, Howell AS, Shen K (2013) An extracellular adhesion molecule complex patterns dendritic branching and morphogenesis. Cell 155: 296-307

763 Dong X, Shen K, Bulow HE (2015) Intrinsic and extrinsic mechanisms of dendritic
764 morphogenesis. Annu Rev Physiol 77: 271-300
765 Driscoll M, Chalfie M (1991) The *mec*-4 gene is a member of a family of
766 *Caenorhabditis elegans* genes that can mutate to induce neuronal
767 degeneration. Nature 349: 588-593
768 Fox K, Wong RO (2005) A comparison of experience-dependent plasticity in the
769 visual and somatosensory systems. Neuron 48: 465-477
770 Ghiretti AE, Moore AR, Brenner RG, Chen LF, West AE, Lau NC, Van Hooser
771 SD, Paradis S (2014) Rem2 Is an Activity-Dependent Negative Regulator of
772 Dendritic Complexity In Vivo. J Neurosci 34: 392-407
773 Gillespie PGW, R. G. (2001) Molecular basis of mechanosensory transduction.
774 Nature 413: 194-202
775 Gobetto MN, Gonzalez-Inchauspe C, Uchitel OD (2021) Histamine and
776 Corticosterone Modulate Acid Sensing Ion Channels (ASICs) Dependent
777 Long-term Potentiation at the Mouse Anterior Cingulate Cortex. Neurosci
778 Behav Physiol 460: 145-160
779 Goodman CS, Shatz CJ (1993) Developmental mechanisms that generate
780 precise patterns of neuronal connectivity. Cell 72 Suppl: 77-98
781 Goodman MB, Sengupta P (2019) How Caenorhabditis elegans Senses
782 Mechanical Stress, Temperature, and Other Physical Stimuli. Genetics 212:
783 25-51
784 Gyorffy BA, Kun J, Torok G, Bulyaki E, Borhegyi Z, Gulyassy P, Kis V, Szocsics
785 P, Micsonai A, Matko J, Drahos L, Juhasz G, Kekesi KA, Kardos J (2018)
786 Local apoptotic-like mechanisms underlie complement-mediated synaptic
787 pruning. Proc Natl Acad Sci U S A 115: 6303-6308
788 Hall DH, Treinin M (2011) How does morphology relate to function in sensory
789 arbors? Trends Neurosci 34: 443-51
790 Halpain S (2018) Avoiding Sibling Conflict: Lessons from Dendrite Self-
791 Avoidance in C. elegans. Neuron 98: 864
792 Harlow HF, Dodsworth RO, Harlow MK (1965) Total social isolation in monkeys.
793 Proc Natl Acad Sci U S A 54: 90-97
794 Hausser M, Mel B (2003) Dendrites: bug or feature? Curr Opin Neurobiol 13:
795 272-283
796 Hedgecock EM, Sulston JE, Thomson JN (1983) Mutations affecting
797 programmed cell deaths in the nematode *Caenorhabditis elegans*. Science
798 220: 1277-1279
799 Hill AS, Ben-Shahar Y (2018) The synaptic action of Degenerin/Epithelial sodium
800 channels. Channels 12: 262-275
801 Holtmaat A, Svoboda K (2009) Experience-dependent structural synaptic
802 plasticity in the mammalian brain. Nat Rev Neurosci 10: 647-658
803 Hu HT, Huang TN, Hsueh YP (2020) KLHL17/Actinfilin, a brain-specific gene
804 associated with infantile spasms and autism, regulates dendritic spine
805 enlargement. J Biomed Sci 27: 103
806 Huang M, Chalfie M (1994) Gene interactions affecting mechanosensory
807 transduction in Caenorhabditis elegans. Nature 367: 467-470

808 Huebschman JL, Corona KS, Guo Y, Smith LN (2020) The Fragile X Mental
809 Retardation Protein Regulates Striatal Medium Spiny Neuron Synapse
810 Density and Dendritic Spine Morphology. Front Mol Neurosci 13: 161
811 Husson SJ, Costa WS, Wabnig S, Stirman JN, Watson JD, Spencer WC,
812 Akerboom J, Looger LL, Treinin M, Miller DM, 3rd, Lu H, Gottschalk A
813 (2012) Optogenetic analysis of a nociceptor neuron and network reveals ion
814 channels acting downstream of primary sensors. Curr Biol 22: 743-752
815 Inberg S, Meledin A, Kravtsov V, Iosilevskii Y, Oren-Suissa M, Podbilewicz B
816 (2019) Lessons from worm dendritic patterning. Annual review of
817 neuroscience 42: 365-383
818 Iosilevskii Y, Podbilewicz B (2021) Programmed cell fusion in development and
819 homeostasis. Curr Top Dev Biol 144: 215-244
820 Jan YN, Jan LY (2010) Branching out: mechanisms of dendritic arborization. Nat
821 Rev Neurosci 11: 316-328
822 Katz EM, Chu DK, Casey KM, Jampachaisri K, Felt SA, Pacharinsak C (2020)
823 The Stability and Efficacy of Tricaine Methanesulfonate (MS222) Solution
824 After Long-Term Storage. J Am Assoc Lab Anim Sci. 12: 393-400
825 Katz LC, Shatz CJ (1996) Synaptic activity and the construction of cortical
826 circuits. Science 274: 1133-1138
827 Kellenberger S, Schild L (2002) Epithelial Sodium Channel/Degenerin Family of
828 Ion Channels: A Variety of Functions for a Shared Structure. Physiol Rev
829 82: 735-767
830 Kim E, Sun L, Gabel CV, Fang-Yen C (2013) Long-Term Imaging of
831 Caenorhabditis elegans Using Nanoparticle-Mediated Immobilization. PLoS
832 One 8: e53419
833 Kolb B, Whishaw IQ (1998) Brain plasticity and behavior. Annu Rev Psychol 49:
834 43-64
835 Kravtsov V, Oren-Suissa M, Podbilewicz B (2017) The fusogen AFF-1 can
836 rejuvenate the regenerative potential of adult dendritic trees via self-fusion.
837 Development 144: 2364-2374
838 Kuhlman SJ, O'Connor DH, Fox K, Svoboda K (2014) Structural Plasticity within
839 the Barrel Cortex during Initial Phases of Whisker-Dependent Learning. J
840 Neurosci 34: 6078-6083
841 Li W, Kang L, Piggott BJ, Feng Z, Xu XZ (2011) The neural circuits and sensory
842 channels mediating harsh touch sensation in Caenorhabditis elegans. Nat
843 Commun 2: 315
844 Luo L (2002) Actin Cytoskeleton Regulation in Neuronal Morphogenesis and
845 Structural Plasticity. Annu Rev Cell Dev Biol 18: 601-635
846 Mango D, Nistico R (2020) Role of ASIC1a in Normal and Pathological Synaptic
847 Plasticity. Reviews of physiology, biochemistry and pharmacology 177: 83-
848 100
849 Maures TJ, Booth LN, Benayoun BA, Izrayelit Y, Schroeder FC, Brunet A (2014)
850 Males shorten the life span of C. elegans hermaphrodites via secreted
851 compounds. Science 343: 541-4

852 Miller-Fleming TW, Petersen SC, Manning L, Matthewman C, Gornet M, Beers A,
853 Hori S, Mitani S, Bianchi L, Richmond J, Miller DM (2016) The DEG/ENaC
854 cation channel protein UNC-8 drives activity-dependent synapse removal in
855 remodeling GABAergic neurons. eLife 5
856 Nagerl UV, Eberhorn N, Cambridge SB, Bonhoeffer T (2004) Bidirectional
857 Activity-Dependent Morphological Plasticity in Hippocampal Neurons.
858 Neuron 44: 759-767
859 Oren-Suissa M, Gattegno T, Kravtsov V, Podbilewicz B (2017) Extrinsic Repair of
860 Injured Dendrites as a Paradigm for Regeneration by Fusion in
861 Caenorhabditis elegans. Genetics 206: 215-230
862 Oren-Suissa M, Hall D, Treinin M, Shemer G, Podbilewicz B (2010) The Fusogen
863 EFF-1 Controls Sculpting of Mechanosensory Dendrites. Science 328:
864 1285-1288
865 Rose JK, Sangha S, Rai S, Norman KR, Rankin CH (2005) Decreased sensory
866 stimulation reduces behavioral responding, retards development, and alters
867 neuronal connectivity in Caenorhabditis elegans. J Neurosci 25: 7159-68
868 Roy Choudhury A, Groflhans J, Kong D (2021) Ion Channels in Epithelial
869 Dynamics and Morphogenesis. Cells 10: 2280
870 Salzberg Y, Diaz-Balzac CA, Ramirez-Suarez NJ, Attreed M, Tecle E, Desbois
871 M, Kaprielian Z, Bulow HE (2013) Skin-Derived Cues Control Arborization
872 of Sensory Dendrites in Caenorhabditis elegans. Cell 155: 308-20
873 Salzberg Y, Ramirez-Suarez NJ, Bulow HE (2014) The proprotein convertase
874 KPC-1/furin controls branching and self-avoidance of sensory dendrites in
875 Caenorhabditis elegans. PLoS genetics 10: e1004657
876 Sawin ER, Ranganathan R, Horvitz HR (2000) C. elegans locomotory rate is
877 modulated by the environment through a dopaminergic pathway and by
878 experience through a serotonergic pathway. Neuron 26: 619-631
879 Shi S, Luke CJ, Miedel MT, Silverman GA, Kleyman TR (2016) Activation of the
880 Caenorhabditis elegans Degenerin Channel by Shear Stress Requires the
881 MEC-10 Subunit. J Biol Chem 291: 14012-14022
882 Shi S, Mutchler SM, Blobner BM, Kashlan OB, Kleyman TR (2018) Pore-lining
883 residues of MEC-4 and MEC-10 channel subunits tune the Caenorhabditis
884 elegans degenerin channel's response to shear stress. J Biol Chem 293:
885 10757-10766
886 Sin WC, Haas K, Ruthazer ES, Cline HT (2002) Dendrite growth increased by
887 visual activity requires NMDA receptor and Rho GTPases. Nature 419: 475-
888 480
889 Smith CJ, Watson JD, Spencer WC, O'Brien T, Cha B, Albeg A, Treinin M, Miller
890 DM, 3rd (2010) Time-lapse imaging and cell-specific expression profiling
891 reveal dynamic branching and molecular determinants of a multi-dendritic
892 nociceptor in C. elegans. Dev Biol 345: 18-33
893 Star EN, Kwiatkowski DJ, Murthy VN (2002) Rapid turnover of actin in dendritic
894 spines and its regulation by activity. Nat Neurosci 5: 239-246

895 Stein IS, Park DK, Claiborne N, Zito K (2021) Non-ionotropic NMDA receptor
896 signaling gates bidirectional structural plasticity of dendritic spines. Cell
897 reports 34: 108664
898 Sulston JE, Schierenberg E, White JG, Thomson JN (1983) The Embryonic Cell
899 Lineage of the Nematode *Caenorhabditis elegans*. Dev Biol 100: 64-119
900 Suzuki H, Kerr R, Bianchi L, Frokjaer-Jensen C, Slone D, Xue J, Gerstbrein B,
901 Driscoll M, Schafer WR (2003) In vivo imaging of C. elegans
902 mechanosensory neurons demonstrates a specific role for the MEC-4
903 channel in the process of gentle touch sensation. Neuron 39: 1015-1017
904 Tao L, Porto D, Li Z, Fechner S, Lee SA, Goodman MB, Xu XZS, Lu H, Shen K
905 (2019) Parallel Processing of Two Mechanosensory Modalities by a Single
906 Neuron in C. elegans. Dev Cell 51: 617-631 e3
907 Tavosanis G (2012) Dendritic structural plasticity. Dev Neurobiol 72: 73-86
908 Tendilla-Beltran H, Antonio Vazquez-Roque R, Judith Vazquez-Hernandez A,
909 Garces-Ramirez L, Flores G (2019) Exploring the Dendritic Spine Pathology
910 in a Schizophrenia-related Neurodevelopmental Animal Model.
911 Neuroscience 396: 36-45
912 Tsalik EL, Niacaris T, Wenick AS, Pau K, Avery L, Hobert O (2003) LIM
913 homeobox gene-dependent expression of biogenic amine receptors in
914 restricted regions of the C. elegans nervous system. Dev Biol 263: 81-102
915 Vaillant AR, Zanassi P, Walsh GS, Aumont A, Alonso A, Miller FD (2002)
916 Signaling mechanisms underlying reversible, activity-dependent dendrite
917 formation. Neuron 34: 985-998
918 Way JC, Chalfie M (1988) mec-3, a homeobox-containing gene that specifies
919 differentiation of the touch receptor neurons in C. elegans. Cell 54: 5-16
920 Welsh MJ, Price MP, Xie J (2002) Biochemical Basis of Touch Perception:
921 Mechanosensory Function of Degenerin/Epithelial Na+ Channels. J Biol
922 Chem 277: 2369-2372
923 Wiesner T, Bilodeau A, Bernatchez R, Deschenes A, Raulier B, De Koninck P,
924 Lavoie-Cardinal F (2020) Activity-Dependent Remodeling of Synaptic
925 Protein Organization Revealed by High Throughput Analysis of STED
926 Nanoscopy Images. Front Neural Circuits 14: 57
927 Wilbrecht L, Holtmaat A, Wright N, Fox K, Svoboda K (2010) Structural Plasticity
928 Underlies Experience-Dependent Functional Plasticity of Cortical Circuits. J
929 Neurosci 30: 4927-4932
930 Wong RO, Ghosh A (2002) Activity-dependent regulation of dendritic growth and
931 patterning. Nat Rev Neurosci 3: 803-812
932 Xu T, Yu X, Perlik AJ, Tobin WF, Zweig JA, Tennant K, Jones T, Zuo Y (2009)
933 Rapid formation and selective stabilization of synapses for enduring motor
934 memories. Nature 462: 915-919
935 Yang G, Pan F, Gan WB (2009) Stably maintained dendritic spines are
936 associated with lifelong memories. Nature 462: 920-924
937 Younger MA, Muller M, Tong A, Pym EC, Davis GW (2013) A Presynaptic ENaC
938 Channel Drives Homeostatic Plasticity. Neuron 79: 1183-1196

939 Yu X, Zuo Y (2011) Spine plasticity in the motor cortex. Curr Opin Neurobiol 21:
940 169-174
941 Zhang Y, Cudmore RH, Lin DT, Linden DJ, Huganir RL (2015) Visualization of
942 NMDA receptor–dependent AMPA receptor synaptic plasticity in vivo. Nat
943 Neurosci 18: 402-407
944 Zhou Z, Hong EJ, Cohen S, Zhao WN, Ho HY, Schmidt L, Chen WG, Lin Y,
945 Savner E, Griffith EC, Hu L, Steen JA, Weitz CJ, Greenberg ME (2006)
946 Brain-Specific Phosphorylation of MeCP2 Regulates Activity-Dependent
947 Bdnf Transcription, Dendritic Growth, and Spine Maturation. Neuron 52:
948 255-269
949 Zuo Y, Yang G, Kwon E, Gan WB (2005) Long-term sensory deprivation
950 prevents dendritic spine loss in primary somatosensory cortex. Nature 436:
951 261-265
952

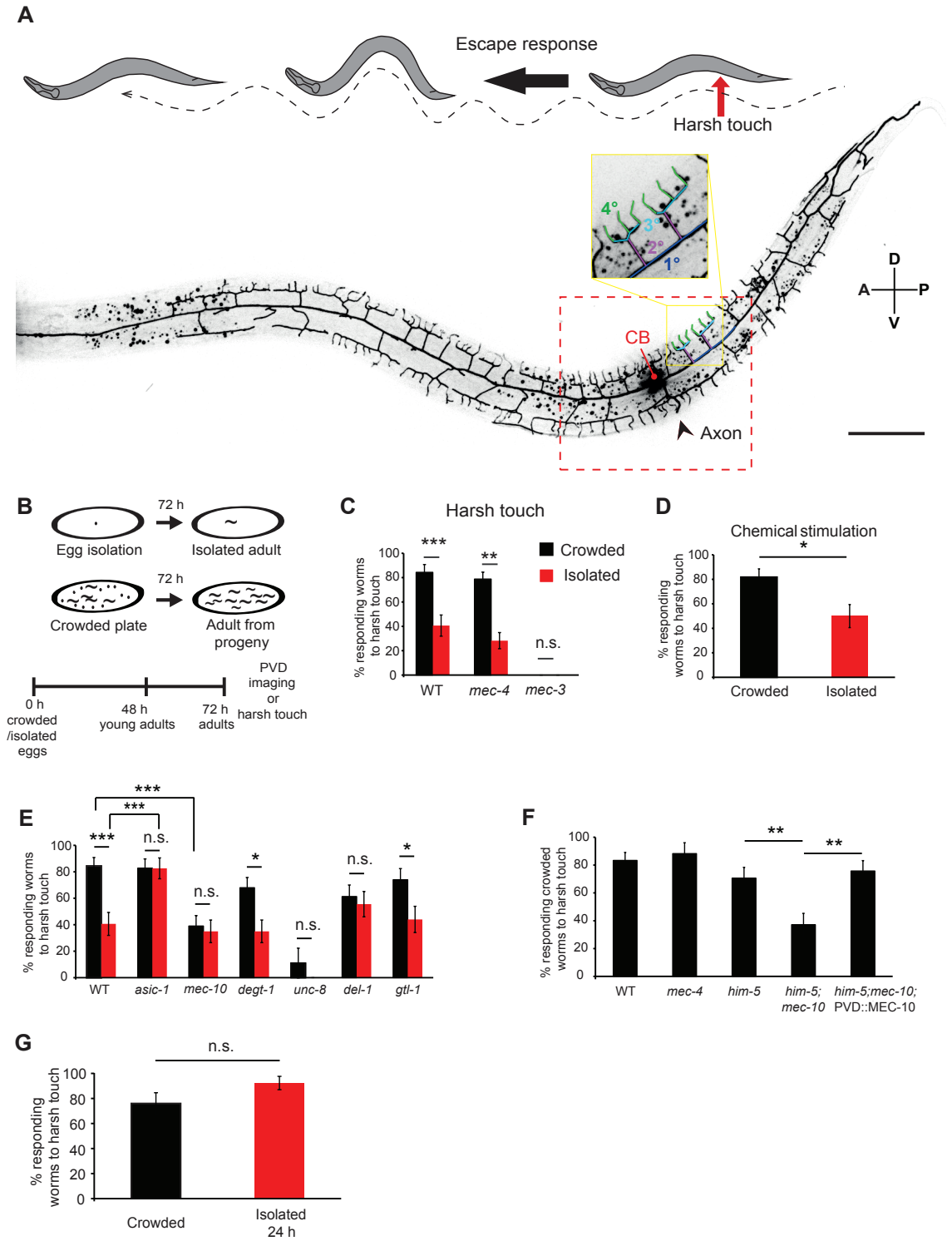

Figure 1. Mechanosensory deprivation during development reduces the behavioral response of the PVD neuron. (A) The PVD neuron dendritic tree, cell body (CB) and axon. The red arrow corresponds to the contact point with a platinum wire during posterior harsh

958 touch, while the black arrow represents the behavioral escape response of the worm. The red
959 dashed square represents the analyzed region around the CB. One representative candelabrum
960 is colored by branch orders: blue primary (1°), purple secondary (2°), cyan tertiary (3°) and
961 green quaternaries (4°). A- anterior; P- posterior; V- ventral; D-dorsal. **(B)** Schematic of the
962 isolation protocol followed at 72 h by posterior harsh touch assay or PVD imaging of adult
963 worms. **(C)** Isolation of embryos reduced the percentage of worms responding to harsh touch at
964 adulthood. Crowded- black bars, Isolated- red bars. Wildtype (WT) N2 worms (Crowded, n=32;
965 Isolated, n=32), *mec-4* (Crowded, n=52; Isolated, n=46), *mec-3* (Crowded, n=12; Isolated,
966 n=12). *mec-4* animals were assayed as adults after 96 h to account for their slower rate of
967 growth. **(D)** Growth in plates with chemical cues from adult hermaphrodites did not alter the
968 reduced response rate of isolated *mec-4* animals to harsh touch (Crowded, n=33; Isolated,
969 n=28). **(E)** Harsh touch response in crowded and isolated conditions for mutants of different
970 DEG-ENaCs and the TRP channel *gtl-1*. WT worms (same set of worms as in Fig. 1C.
971 Crowded, n=32; Isolated, n=32), *asic-1* (Crowded, n=46; Isolated, n=30), *mec-10* (Crowded,
972 n=38; Isolated, n=31), *degt-1* (Crowded, n=37; Isolated, n=31), *unc-8* (Crowded, n=18; Isolated,
973 n=15), *del-1* (Crowded, n=31; Isolated, n=27), *gtl-1* (Crowded, n=27; Isolated, n=25). **(F)** MEC-
974 10 expression in the PVD rescues *mec-10* mutants' crowded-specific reduction in response to
975 harsh touch. All strains contain the *ser-2Prom3::Kaede* PVD marker construct, and were tested
976 in the crowded conditions. (WT, n=42; *mec-4,* n=17; *him-5,* n=34 (*him-5* was used as WT
977 background for several strains after cross); *him-5;mec-10,* n=35; *him-5;mec-*
978 *10*;*ser2Prom3*::MEC-10, n=33). **(G)** Isolation for 24 h in adulthood did not affect the response to
979 harsh touch. Worms grown under crowded conditions were isolated for 24 h as young adults
980 and compared against their crowded age-matched counterparts in their response to harsh touch
981 (Crowded, n=25; Isolated for 24 h, n=26). The proportion of responding worms (percentage) ±
982 standard error of proportion is shown. Fisher's exact test, *p<0.05, **p<0.01, ***p<0.001, n.s.
983 not significant.
984

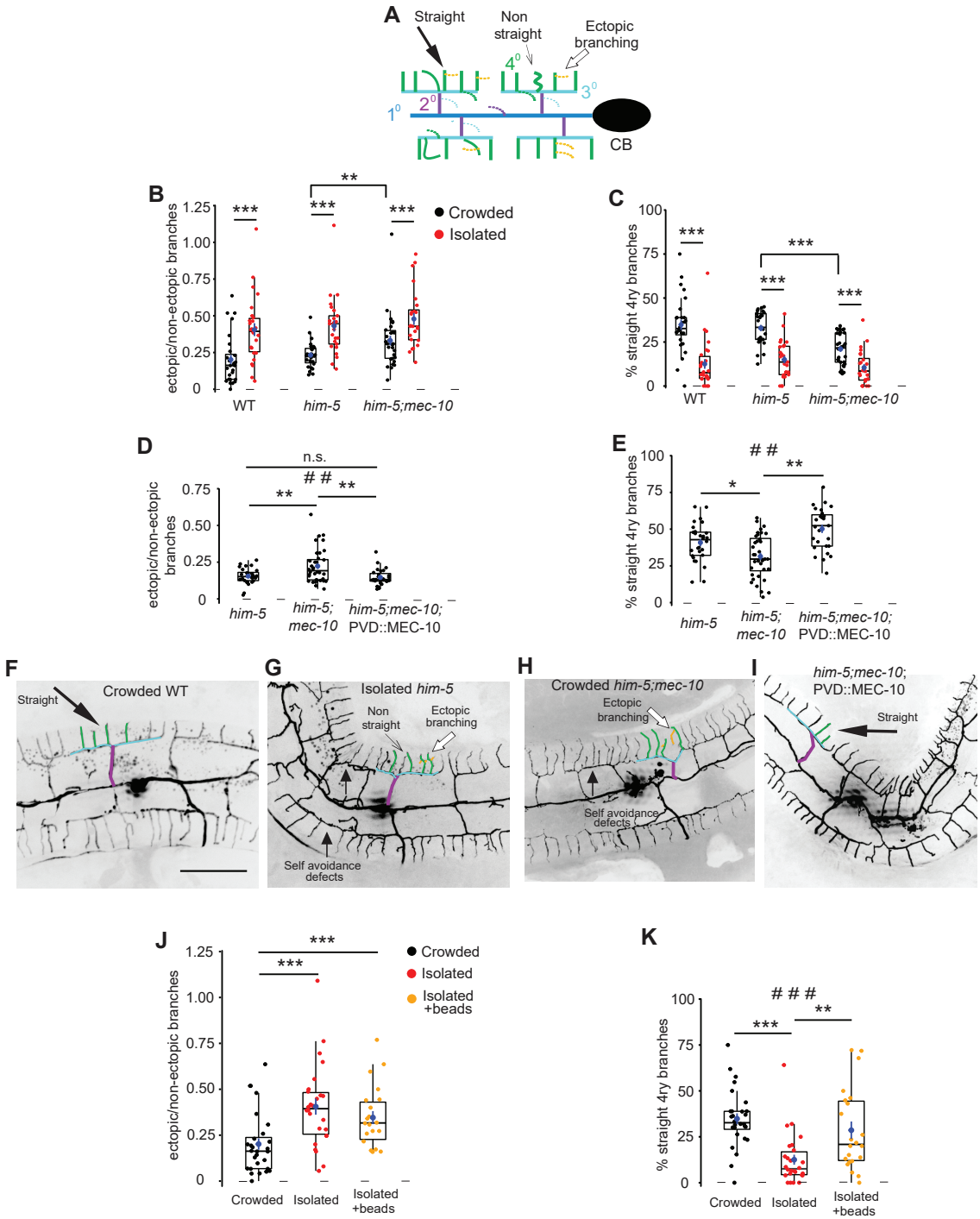

Figure 2. Mechanosensory deprivation and cell autonomous activity of *mec-10* affects the architecture of the PVD. (A) Schematic representation of the PVD dendritic structure, marking the morphological characteristics of interest: ectopic branches and quaternary branching geometry. Dashed lines represent ectopic branching at each order. Colors correspond to Fig. 1A. (**B-G**) Both isolation and *mec-10* affect the structure of the PVD: **(B)** Isolation increases the

992 fraction of ectopic branching, *mec-10* mutation increases ectopic branching in the crowded
993 state. **(C)** Isolation decreases the percentage of straight quaternary branches, *mec-10* mutation
994 decreases the percentage of straight quaternary branches in the crowded state. Crowded- black
995 dots, isolated- red dots; WT (Crowded, n=28; Isolated n=26), *him-5* (Crowded, n=27; Isolated,
996 n=25; *him-5* was used as WT background for several strains after cross), *him-5;mec-10*
997 (Crowded, n=30; Isolated, n=24). **(D)** Expression of *mec-10* in the PVD on the background of
998 *him-5;mec-10* in the crowded state reduces ectopic branching and **(E)** increases the percentage
999 of straight quaternary branches. **(F-I)** Representative PVD images of WT, *mec-10* and *mec-*
1000 *10*;PVD::MEC-10 in different growth conditions. (Scale bar, 50 μm). **(J)** Embryo isolation with
1001 glass beads did not affect ectopic branching. **(K)** Embryo isolation with glass beads increased
1002 the percentage of straight quaternary branches (Crowded, n=28; Isolated n=26; Isolated with
1003 beads, n=22. Crowded and isolated WT are the same set of worms as in Fig. 2B,C). Each dot
1004 represents a single worm. The mean ± s.e.m. are shown in blue. Box plot with median and
1005 hinges for the first and third quartile. The whiskers represent an estimated calculation of the
1006 95% confidence interval. Kruskal-Wallis test, # # $p<0.01$, # # # $p<0.001$, Mann Whitney test with
1007 Bonferroni Correction $\alpha=0.0167$. *$p<0.05$, ** $p<0.01$, *** $p<0.001$, n.s. not significant.
1008

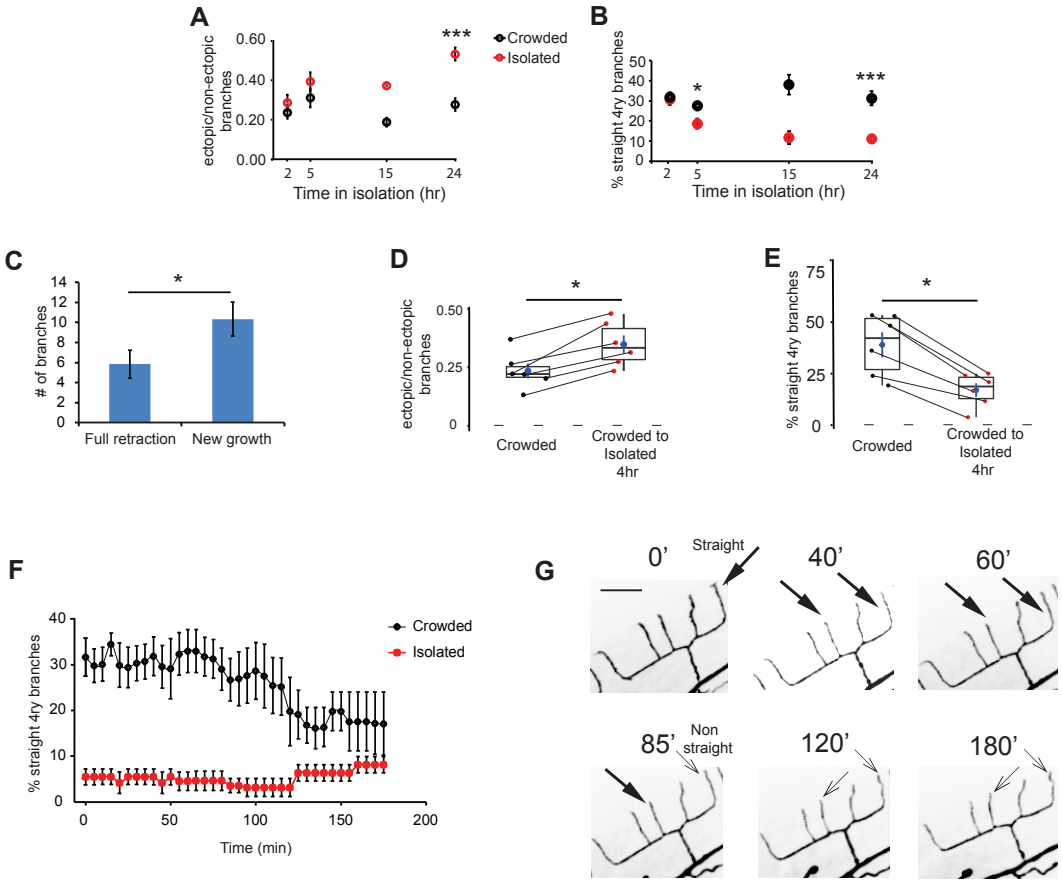

Figure 3. Adult isolation for less than 4 h affects the structure of the PVD.
(A) Isolation of crowded worms induces a time-dependent increase in the proportion of ectopic branches, and **(B)** a decrease in the number of straight quaternary branches (2 h: Crowded, n=24, Isolated, n=22; 5 h: Crowded, n=24, Isolated, n=27; 15 h: Crowded, n=3, Isolated, n=3; 24 h: Crowded, n=20, Isolated, n=21; animals imaged using polystyrene beads for immobilization, see Materials and Methods). **(C)** Isolation for 4 h induces more growth of new branches than retraction of existing ones. Ectopic branch dynamics were compared for crowded animals against their state after 4 h isolation. Imaging used 1% tricaine, see Materials and Methods. **(D)** Isolation of crowded worms for 4 h increases the ratio between ectopic/non-ectopic branches in individual animals and **(E)** reduces the percentage of straight quaternary branches (Crowded, n=6; Isolated n=6). **(F)** Crowded, but not isolated worms, show dynamic reduction in the percentage of straight quaternary branches during a 3 h time lapse movie in 1% tricaine; see Movies S1 and S2. **(G)** Representative time lapse frames of a crowded worm in 1% tricaine. Thick and thin arrows represent straight and non-straight quaternary branches, respectively. For **(D, E)** the lines connecting two points refer to the same crowded specimen at time 0 and after 4 h isolation. Box plot representation as in Fig. 2. For **(A-B)** Mann-Whitney test, * $p<0.05$,.*** $p<0.001$. For **(C-E)** Wilcoxon test (for two related samples), * $p<0.05$. The mean ± s.e.m. are shown for panels A-C, and F.

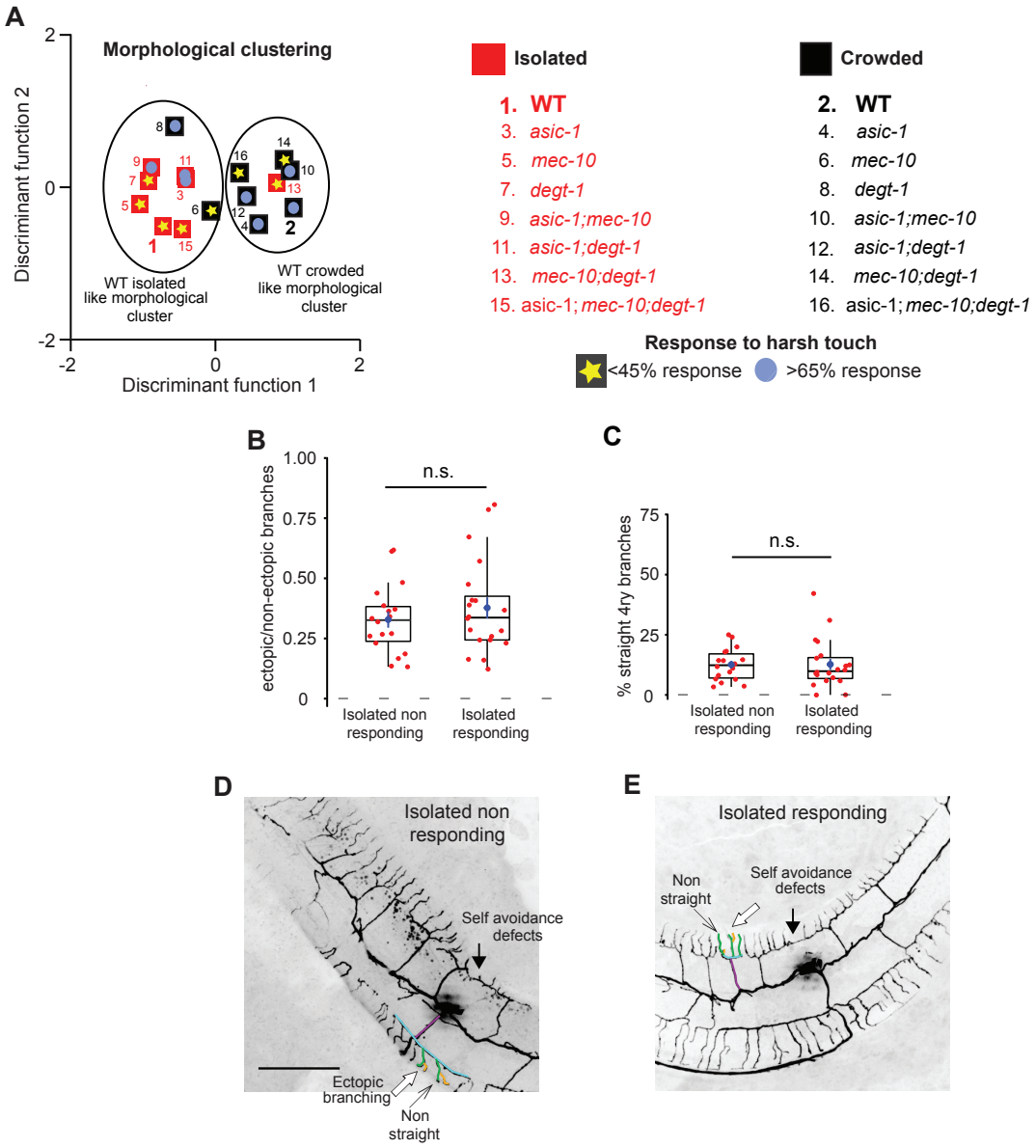

Figure 4. Response to harsh touch and PVD morphology are independent.
(A) Discriminant analysis shows independence of harsh touch response from the PVD's morphological classification. Squares indicate the centroids for morphological characteristics analyzed in Fig. S10A-C. The response to harsh touch (Fig. S9) is illustrated by its magnitude (low, <45% in yellow star; high, >65% in light blue circles). The different genotypes are numbered in the list on the right. Crowded- black, Isolated- red. **(B-E)** Isolated animals show similar PVD morphology regardless of their touch response: **(B)** isolated responding and non-responding animals are not different with regard to the fraction of ectopic branching, and **(C)** the geometry of quaternary branches (Isolated non-responding, n=18; Isolated responding, n=20). Box plot representation as in Fig. 2. Mann-Whitney test. n.s. not significant. **(D, E)** Representative PVD images of responding and non-responding worms. (Scale bar, 50 μm).

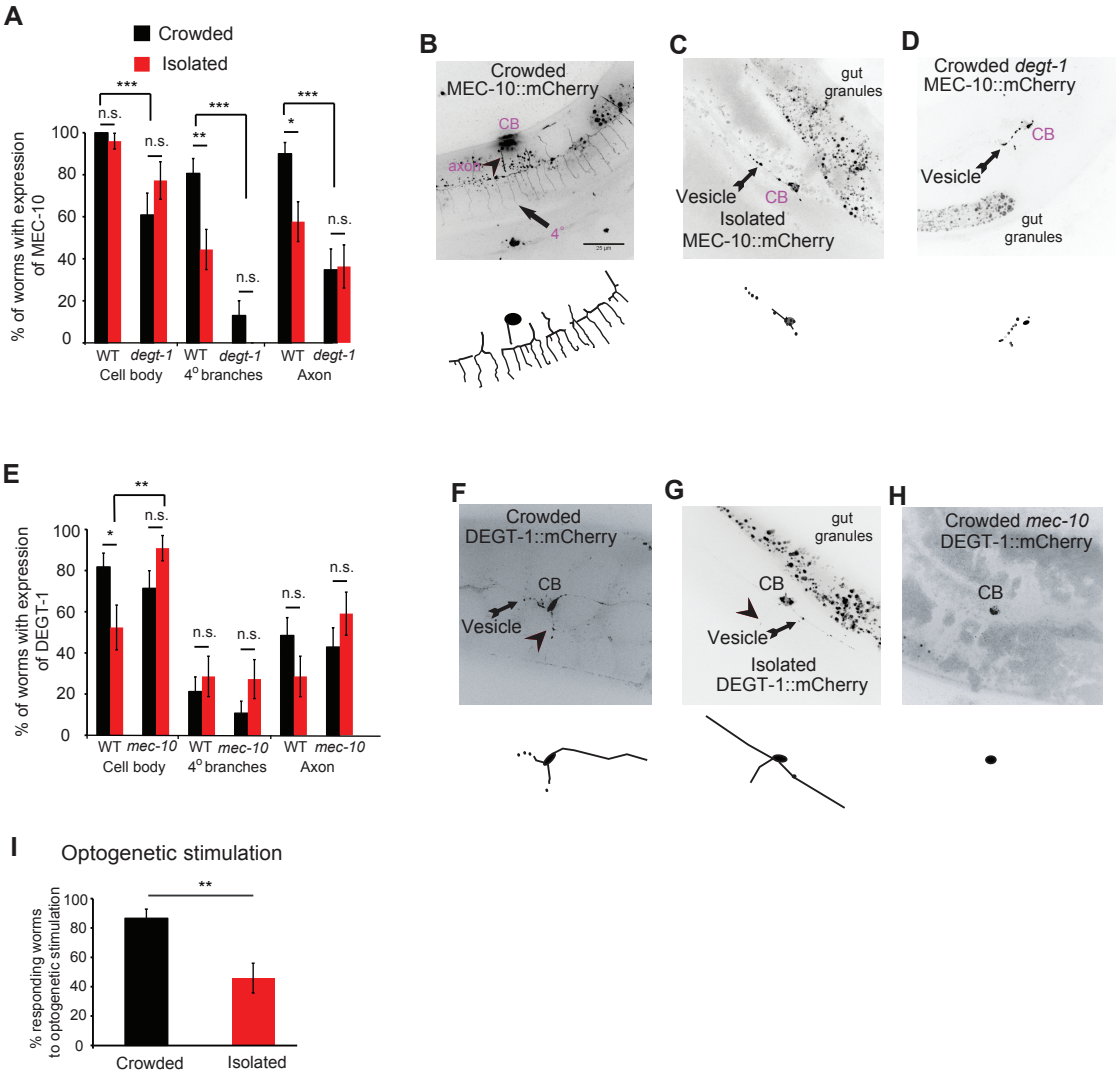

Figure 5. Mechanosensory-dependent localization of degenerins and optogenetics. (A) PVD::MEC-10::mCherry localization (shown and labeled in purple, also in Fig. 7) is reduced in the quaternary branches and the axon following isolation, in a *degt-1*-dependent manner (WT: Crowded, n=31; Isolated, n=27; *degt-1* mutants: Crowded, n=23; Isolated, n=22). **(B-D)** Representative images and reconstructions for PVD::MEC-10::mCherry localization for crowded and isolated WT worms, and crowded *degt-1* worms. (Scale bar, 50 µm). **(E)** PVD::DEGT-1::mCherry localization level is reduced at the cell body, but not in the quaternary branches or the axon, following isolation, in a *mec*-10-dependent-manner (WT: Crowded, n=33; Isolated, n=21; *mec-10* mutants: Crowded, n=28; Isolated, n=22). The percentage of expressing worms ± standard error of proportion is shown. **(F-H)** Representative images and reconstructions for PVD::DEGT-1::mCherry localization for crowded and isolated WT worms and crowded *mec-10* worms. **(I)** Isolation leads to a reduced escape response following optogenetic photoactivation of Channelrhodopsin 2 in the PVD (Crowded, n=30; Isolated, n=24, grown on All Trans Retinal. No response was observed for worms grown without All Trans Retinal). Fisher exact test, *p<0.05, **p<0.01, ***p<0.01 n.s. not significant.

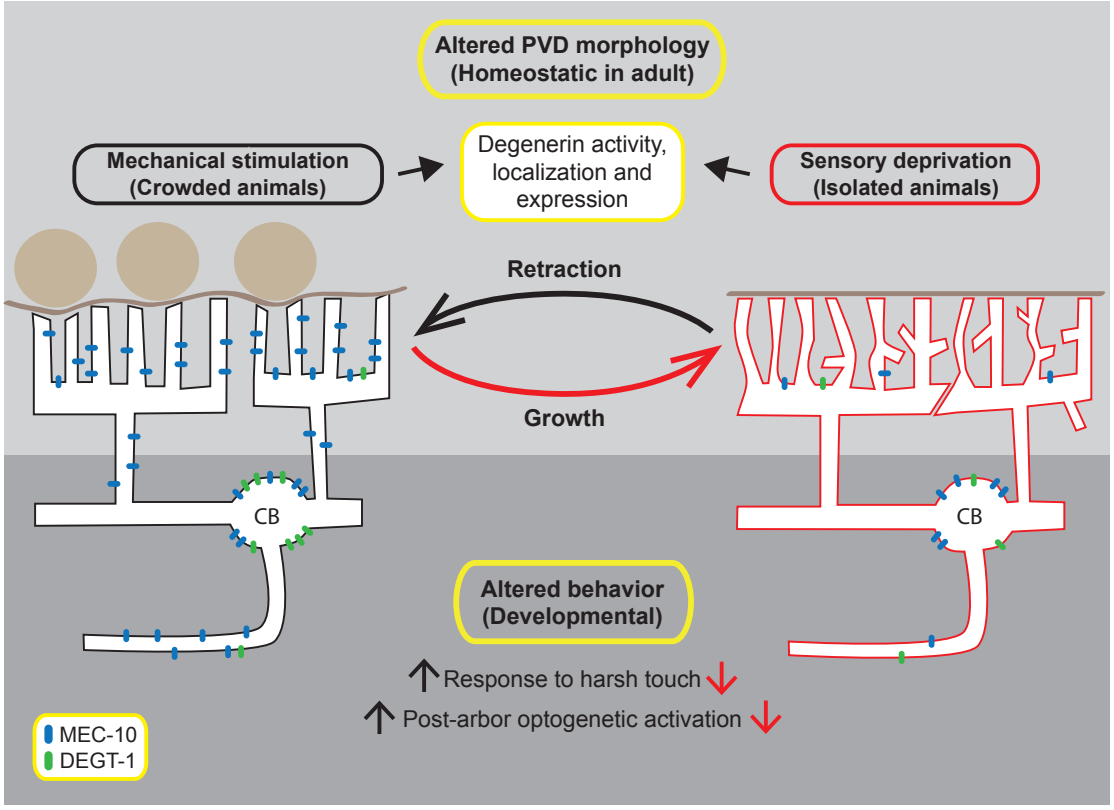

Figure 6. Model of experience-induced structural and behavioral plasticity. During adulthood, mechanosensory signals maintain the structure of the PVD in crowded animals, with straight quaternary branches and fewer ectopic branches. Sensory deprivation (in isolated animals) results in ectopic dendrites, wavy branches and defects in candelabra self-avoidance. During development, mechanosensory experience alters the response to harsh touch and the crawling gait of the worm, possibly through changes in MEC-10 localization in the axon and mediated by other DEG/ENaCs. Mechanosensory stimuli are a driving force for changes in the compartment specific localization of MEC-10 and DEGT-1 in the PVD, which may affect the structure of the PVD. MEC-10 is represented in blue, DEGT-1 is represented in green.